Thin-Walled Structures 55 (2012) 1–10

Contents lists available at SciVerse ScienceDirect

Thin-Walled Structures

journal homepage: www.elsevier.com/locate/tws

Prediction of vacuum-induced buckling pressures of thin-walled cylinders

C. de Paor [a], D. Kelliher [a,*], K. Cronin [b], W.M.D. Wright [c], S.G. McSweeney [c]

[a] Department of Civil and Environmental Engineering, University College Cork, Cork, Ireland
[b] Department of Process and Chemical Engineering, University College Cork, Cork, Ireland
[c] Department of Electrical and Electronic Engineering, University College Cork, Cork, Ireland

ARTICLE INFO

Article history:
Received 14 December 2010
Received in revised form
1 March 2012
Accepted 1 March 2012

Keywords:
Thin shells
Buckling
Geometric imperfections
Uniform external pressure
Finite element analysis

ABSTRACT

The effect of geometric imperfections on the buckling capacity of thin cylindrical shells subjected to uniform external pressure is investigated in this paper. Geometric surveys were conducted on small-scale thin cylinders in order to measure geometric imperfections of the shell surface. These imperfections were then modelled in the FE analysis and a geometrically nonlinear static analysis was carried out. The cylinders are tested to collapse in the laboratory and the results are compared to the results of the FE analysis. Both collapse pressure and postbuckling mode shape are accurately predicted by the FE analysis.

1. Introduction

Thin cylindrical shells are very efficient structures and have a wide range of uses. They are found in the aerospace industry for airplane fuselages, structural engineering applications, in the oil and gas industries for piping and storage of fluids, ship hulls, and in the process sector for the transport of fluids by road tanker and for general liquid storage. Thin-walled cylindrical tanks are prone to buckling collapse due to accidentally induced internal vacuum. While internal under-pressures can be generated for a variety of reasons, the condensation of steam in the vessel results in a particularly rapid and severe level of vacuum loading. The particular motivation for this research is tank collapse or pressure vessel failure in the food, pharmaceutical and biotechnology industries. These vessels are routinely filled with saturated steam as part of cleaning, sterilisation or purging cycles. Condensation of the steam if accompanied by inadvertent closure of all vessel valves will lead to a rapid drop in internal pressure and vessel failure. Such a collapse, if it occurs, tends to be catastrophic resulting in the complete destruction of the vessel. Notwithstanding that the basis of this type of failure is understood and can be averted by proper vessel design and operating procedures, it is still a regular occurrence, as illustrated in Fig. 1.

Calculating buckling loads and predicting postbuckling mode shapes are deemed to be two of the most challenging problems in engineering. These problems are extremely sensitive to external factors and highly nonlinear at the point of bifurcation, leading to difficulty determining critical pressures and postbuckling mode shapes. Thus, much research has been dedicated to investigating the factors affecting vessel collapse [2–6]. Studies have shown that vast discrepancies exist between experimental results and predicted theoretical values with experimental results falling between 10% and 80% of the predicted values. Fig. 2, taken from an early paper by Weingarten et al. [7], shows values for the experimental buckling pressure P, divided by the theoretical buckling pressure P_{cl}, versus the radius/thickness ratio R/h. It is clear that all values fall well below 1.0 (where predicted and experimental collapse pressure values are equivalent) and in fact many values fall under 0.3 (experimental value 30% of that predicted). Since the buckling load is dependent on shell geometry and in particular the L/r (length to radius) and R/t (radius to thickness) ratios, it is widely accepted that these discrepancies are due to the highly sensitive nature of the shells to geometric and material imperfections [8]. Geometric imperfections comprise any geometrical feature of the shell which alters it from a perfect shell. These can include out-of-roundness or ovality [9], wall thickness variation [2], welded seams [10] or other random geometric imperfections such as dents [11]. Material imperfections such as anisotropy may also reduce buckling capacity. Some studies have investigated the effect of geometric imperfections on buckling capacity either experimentally [12–14] or numerically [15,16], but few have compared experimental results to nonlinear

* Corresponding author.
E-mail addresses: c.depaor@umail.ucc.ie (C. de Paor), d.kelliher@ucc.ie (D. Kelliher).

0263-8231/$ - see front matter © 2012 Elsevier Ltd. All rights reserved.
doi:10.1016/j.tws.2012.03.001

Fig. 1. Example of pressure vessel collapse due to plastic sheet blocking vent [1].

finite element (FE) analyses that include the geometric imperfections [17,18]. This is the primary aim of this paper.

An Initial Imperfection Data Bank [4] was set up in the 1980s containing results of several imperfection surveys of shells. Researchers may contribute their own data or use the existing data in numerical analysis with the aim of improving design standards. This led to several studies on the effect of initial imperfection on buckling capacity including analysis on shells subjected to axial loading [19–21]. Studies on other geometric imperfections have also been carried out such as variation in shell thickness investigated by Aghajari et al. [2], the effect of presence of a dent in addition to initial imperfection on the buckling capacity carried out by Guggenburger [11] and Park and Kyriakides [22], and the influence of welds on buckling capacity examined by Teng [23].

Sophisticated methods of nonlinear analysis that allow the user to include for these imperfections exist for this type of

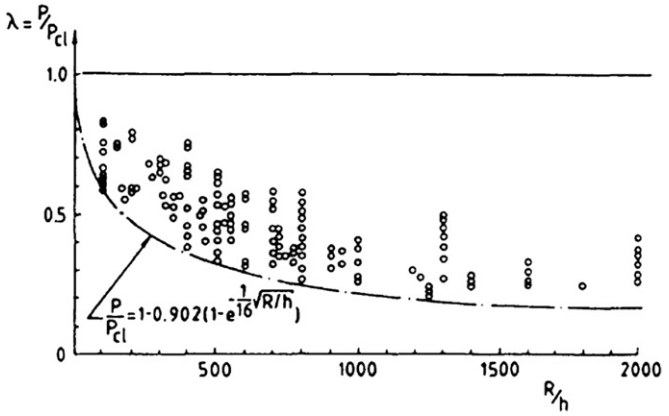

Fig. 2. Distribution of buckling test data for cylinders with closed ends subjected to axial compression, from Weingarten et al. [7].

problem but the difficulty of accurate buckling load prediction persists. This study focuses on the effect of manufacturing-induced geometric imperfections on the buckling of thin cylindrical shells under uniform vacuum. The geometric imperfections of small-scale steel cans are measured and subsequently modelled in FE. These cans are then tested in the laboratory with the results compared to those predicted by the FE analysis.

2. Buckling theory

Buckling is one of the most complex structural analysis problems and buckling loads remain difficult to accurately predict. A combination of axial loads and external pressure is typical in machine design, ship building or tanks used in chemical engineering. If a cylinder is loaded with a uniform hydrostatic pressure such as this, a bifurcation point will be reached where the net external pressure on the vessel exceeds a critical pressure, P_c. At this point, sudden or 'snap-through' radial buckling will occur. There are a number of approaches to obtain values for P_c; the most frequently used being the equilibrium method. The equilibrium method is based on the observation that at a critical load, a deformed state of a shell exists that is assumed to be close to its initial unbuckled state of equilibrium. Thus, the appearance of a possible bifurcation in the solution corresponds to the critical load. This criterion for determining critical loads can be used to obtain the governing differential equations of the shell buckling analysis [24]. This method may be employed when an axial load is present in addition to external lateral pressure, as in this case. Von Mises [3] solved this for a cylindrical shell with closed end subjected to the action of a uniform hydrostatic pressure obtaining the following expression:

$$P_c = \frac{Et}{r}\left(\frac{1}{n^2+\frac{1}{2}\left(\frac{\pi r}{l}\right)^2}\right)\left(\frac{1}{\left(n^2\left(\frac{l}{\pi r}\right)^2+1\right)^2} + \frac{t^2}{12(1-\nu^2)r^2}\left(n^2+\left(\frac{\pi r}{l}\right)^2\right)^2\right) \quad (1)$$

As can be seen from Eq. (1), the critical buckling pressure is primarily dependent on the vessel geometry, and in particular, the t/r (thickness to radius) ratio. It is also directly proportional to

Young's modulus of the material. The critical pressure is also dependent on the number of circumferential half-waves, or lobes, n, formed during the buckling process, with a minimum buckling pressure occurring at a specific value of n. n is dependent on vessel geometry, and can be taken from the chart in Fig. 3 developed by Windenburg and Trilling [25]. It is evident from the chart that the number of circumferential waves which form as the shell buckles increases as the length and thickness of the shell decrease. The value of n may also be calculated as the value which gives a minimum for P_c. For the geometry used in this research a value of $n=8$ is expected.

3. Imperfection measurement

To model real geometric imperfections precisely and accurately, measurements of 39 small-scale steel cans were recorded using a custom-built rig. The can walls were cut from thin sheets of steel which have been rolled to a specific thickness. These are then bent into a circular shape and the ends are welded together to form a hollow cylinder. The ends of the can are stamped out of thicker sheets of steel and then added by a method of folding. These cans contain imperfections typical of those caused inadvertently by the manufacturing process similar to those present in larger scale cylinders and tanks and so are suitable for this study. The cans were centred and secured on a base plate which rotated 360°, and four dial gauges, accurate to ± 5 μm, moved vertically on a linear actuator. Three of the dial gauges (Nos. 1–3) were positioned at 120° intervals outside the can with the fourth on the interior, directly opposite gauge No. 1. A schematic of the rig set-up is given in Fig. 4. The base plate was rotated at 2.5° intervals, and after each complete rotation of 360°, the sensors moved vertically downwards in increments of 5 mm. This procedure was repeated until the entire surface area of the can had been measured with a total of 5760 measurements per sensor. In this manner, full geometric information including the thickness variation for each can is produced. Fig. 5 shows the measurement rig set-up.

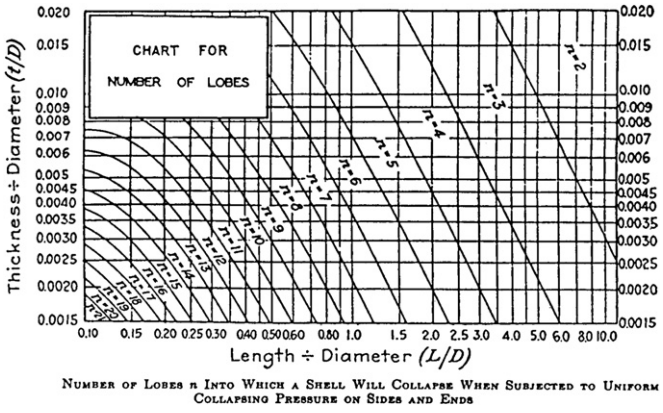

Fig. 3. Chart for number of lobes [25].

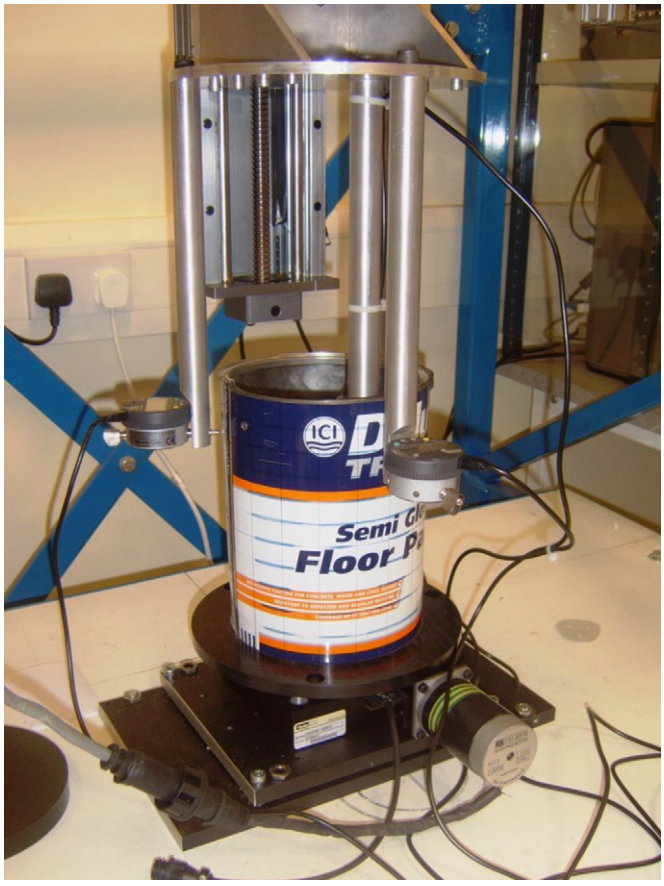

Fig. 5. Can measurement rig.

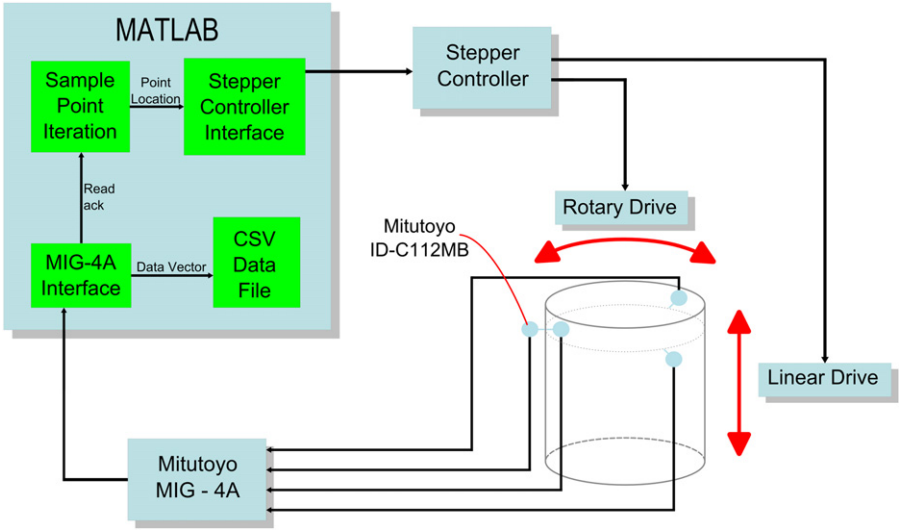

Fig. 4. Measurement rig schematic.

Imperfection in the measurement rig could not be measured *a priori* so that the measurement redundancy was used to determine the systemic errors in the testing rig. Two sensors would have been adequate to record the surface and thickness imperfections; however, the extra sensor readings were used to eliminate these systemic errors from the data. Firstly, due to the minor geometrical differences between cans, the alignment of the can wall was not always parallel to the vertical movement of the linear actuator. This lead to a distortion of the data which was evident on comparison of readings taken from different gauges. Also, the positioning of the centre of the can on the base plate produced an error since it was not exactly on the centre of rotation of the base plate. Once these errors were evaluated and quantified numerically, the data was corrected accordingly. Figs. 6–10 show the surface plots generated in MATLAB for each of the five cans used in testing. The top of the can is at axial = 0 mm with the bottom at axial = 200 mm. The seam is positioned at the same place in each of the plots at circumference = 0 mm. The shape of the can surfaces and the imperfections present on each can are evident from these surface plots. There is a global minimum at around 180° which exists in all the plots. This

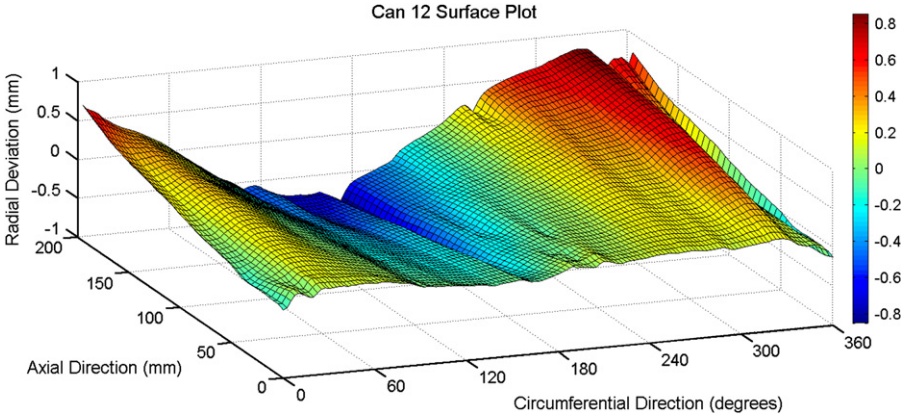

Fig. 6. Surface plot of Can 12.

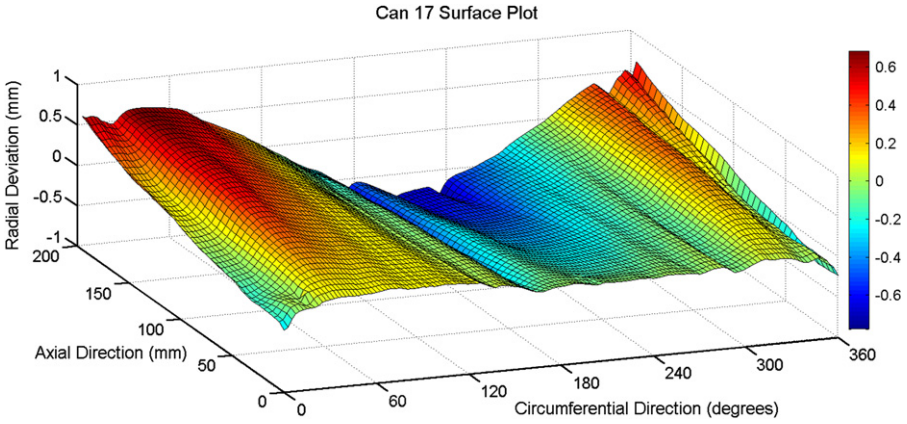

Fig. 7. Surface plot of Can 17.

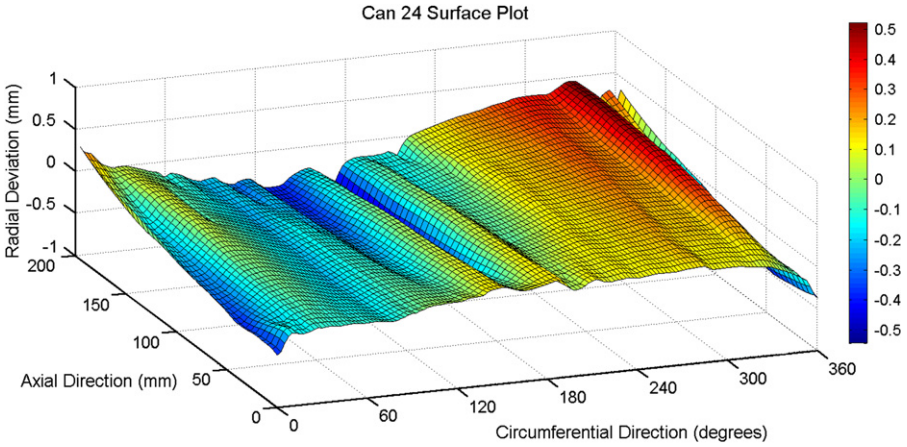

Fig. 8. Surface plot of Can 24.

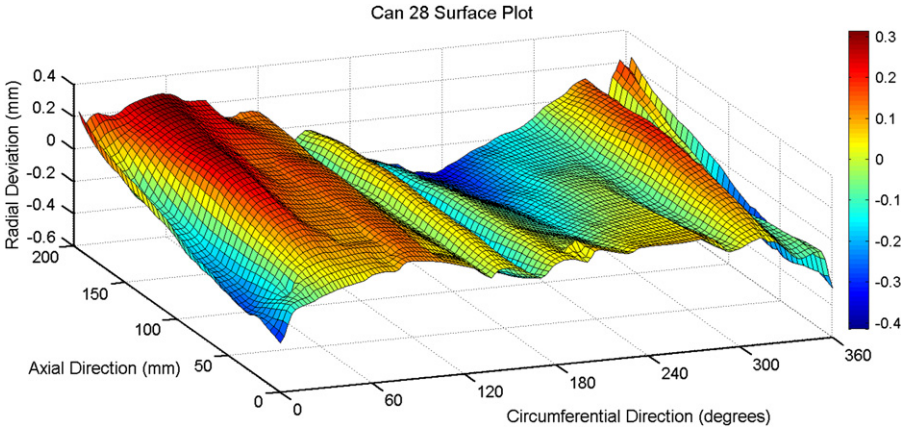

Fig. 9. Surface plot of Can 28.

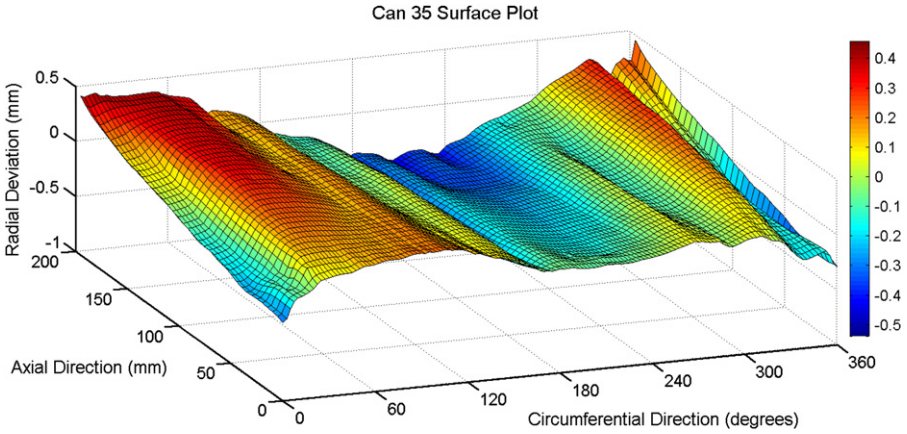

Fig. 10. Surface plot of Can 35.

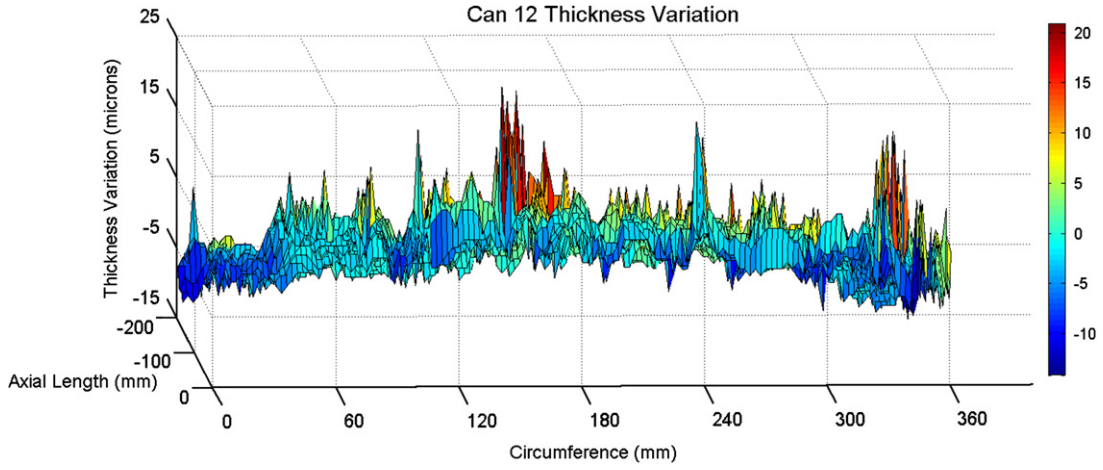

Fig. 11. Thickness variation of Can 12.

flattening is possibly a result of rolling or bending in the manufacturing process. The collected data was then used in the generation of accurate geometric models for the FE analysis of each of the cans.

The thickness variation around the can was also investigated. This was done using the readings from gauge No. 1 and gauge No. 4. Since the gauges were directly opposed, the thickness variation could be evaluated as the difference in readings at each point. Fig. 11 shows this for Can 12. A regression analysis was carried out on the thickness variation and it was found to vary quadratically with the thinnest region near the position of the weld, and the thickest region directly opposite this at 180°. The thickness variation between the maximum and minimum points was found to be about 10 μm and this variation was modelled in the FE analysis.

4. Numerical analysis

In order to determine the buckling pressure of these imperfect shells, finite element analysis is carried out using the data from

the imperfection measurements. The general-purpose finite element analysis system Strand7 is used [26]. A mesh convergence study was carried out initially to determine the mesh requirements.

4.1. Mesh convergence study

For shell buckling analysis, it is widely accepted that in order to accurately model the buckling mode shapes, the minimum number of elements required is two per half wavelength [27]. Therefore, for our analysis 32 elements would have been sufficient in the circumferential direction for a maximum number of eight lobes expected in the circumferential direction (see Section 2). A mesh convergence study with several mesh densities was carried out using the Linear Buckling solver. Results given in Table 1. Song et al. [28] recommend using a mesh density fine enough so that doubling the density of the mesh would not change results more than 1%. In this case, a mesh density of 10×72 elements in the axial and circumferential directions respectively would be sufficient as seen from results in Table 1 and Fig. 12. However, in order to fully represent the geometric imperfections in our model, it was decided that one node would be used to represent each point where a measurement was taken in the measurement surveys, thus giving a total of 145 nodes or 72 shell elements in the circumferential direction and 23 shell elements in the axial direction. This greater number of elements would increase computational costs, however, the geometric imperfections would be represented exactly and output accuracy would be increased.

Table 1
Mesh convergence study.

No. of elements in axial direction	No. of elements in circumferential direction	Total no. of elements	Total degrees of freedom	Numerical buckling pressure (kPa)	% Difference
10	18	180	756	32.46	13.38
10	36	360	1512	29.01	1.33
10	72	720	3024	28.68	0.17
20	36	720	2952	28.99	1.26
20	72	1440	5904	28.66	0.10
23	72	1656	6768	28.66	0.10
20	144	2880	11 808	28.63	0.00

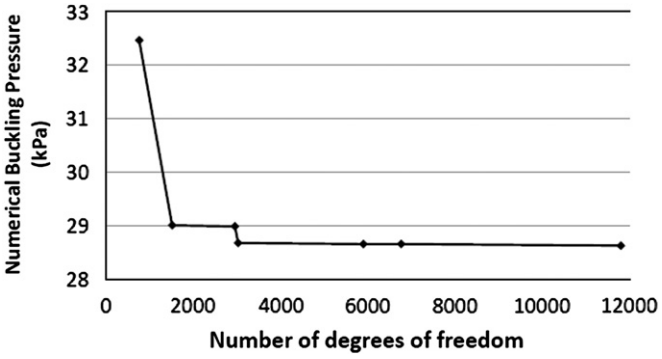

Fig. 12. Mesh convergence graph.

Table 2
Nominal can dimensions, in mm.

Height	Thickness	Radius
230	0.22	88.2

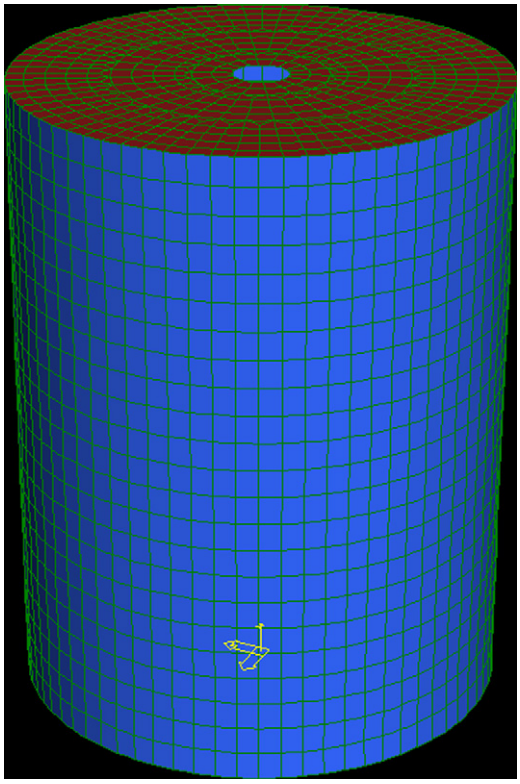

Fig. 13. FE model of can.

Fig. 14. Experimental set-up with can in place.

Table 3
Analytical, numerical and experimental results.

Can no.	Analytical (kPa)	Non-linear FE analysis (kPa)	Experimental (kPa)	% Difference (FE – Exp.)
28	23.17	20.40	20.31	0.44
17	23.17	20.14	20.86	3.45
35	23.17	20.50	21.37	4.24
12	23.17	20.60	21.70	5.34
24	23.17	22.24	19.93	10.38
Mean	23.17	22.7	20.83	4.77

4.2. Model set-up

The model mesh was set up with approximately one node for each reading taken on the can. Rectangular nine-noded quadrilateral shell elements based on Kirchoff's plate theory were used with six degrees of freedom at each node; three translational and three rotational. These nine-noded quadrilateral shell elements were chosen for their accuracy in representing the curved geometry of the shell. Translation in the axial (Z) direction was prevented by restraining the nodes at the bottom of the can where the can wall meets the base at $z=0$ and $R=r$. In addition, translation of one of these nodes was restrained in the X and Y directions and in another node in just the Y direction to ensure no rigid body movement.

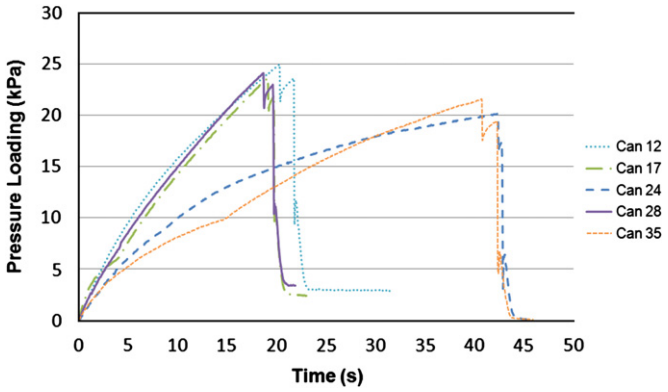

Fig. 15. Pressure histories from experiments of all cans.

Fig. 16. Deformed can after testing.

Tensile tests were carried out on several samples of material from previously collapsed cans to establish the tensile strength of the material. Young's modulus was found to be 205 GPa. The temperature at which the experiment is conducted at varies from 20 °C to 100 °C. Young's modulus of our material (steel) is assumed constant over this temperature range. Poisson's ratio is taken to be 0.03. Dimensions of the can are modelled based on measurements taken shown in Table 2. These values represent nominal dimensions for a perfect shell. The longitudinal welded seam on the can was modelled using a three-noded beam element with six degrees of freedom at each node; three translational and three rotational. This preserved C^1 continuity between the beam element and the two attached nine-noded isoparametric elements. The material properties of the weld are the same as those of the can wall. The width of the beam is taken to be 1.0 mm. The thickness of the seam is found to be twice the thickness of the can wall, 0.44 mm. The weld width is modelled by connecting the beam to the adjoining plate elements using rigid links at each node. The can wall plates were modelled with a thickness variation as shown in Fig. 11 also based on the measured data. The ends of the can were modelled with a thickness of 1 mm replicating their higher thickness. The ends are also modelled with a circular hole of 10 mm radius in the centre where the steam inlet and outlet pipes enter and exit the can in the experiments. There were no restraints applied to the edge elements of the circular holes in the end plates. This replicates the real cylinder geometry where they are free to move. The FE model used is shown in Fig. 13.

FE models replicating the real cans were thus generated and geometrically nonlinear static analyses were carried out to determine the buckling pressures. The nonlinear analysis uses the arc length method for iterative step control. In this approach, the load is applied incrementally and the arc length method searches along the equilibrium path, using a computed positive or negative load factor based on a balance of load and displacement in the increment. It ensures a more stable solution process and can model bifurcation events such as mode jumping and snap-through.

A sensitivity study was conducted to investigate the effect of the end connection on the buckling pressure. A three-noded beam element was modelled around the circumference of the cylinder

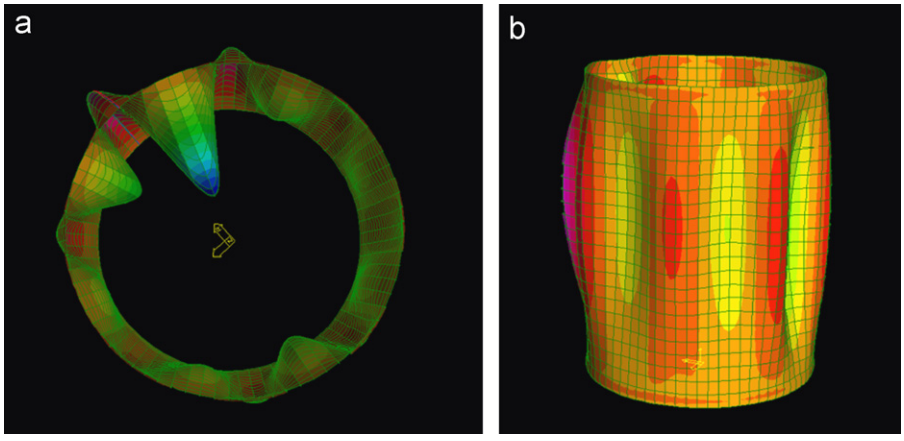

Fig. 17. Deformed shape predicted by the FE analysis in elastic buckling stage. (a) shows plan view and (b) shows elevation. The can ends are removed for visual clarity. Displacements 25 ×.

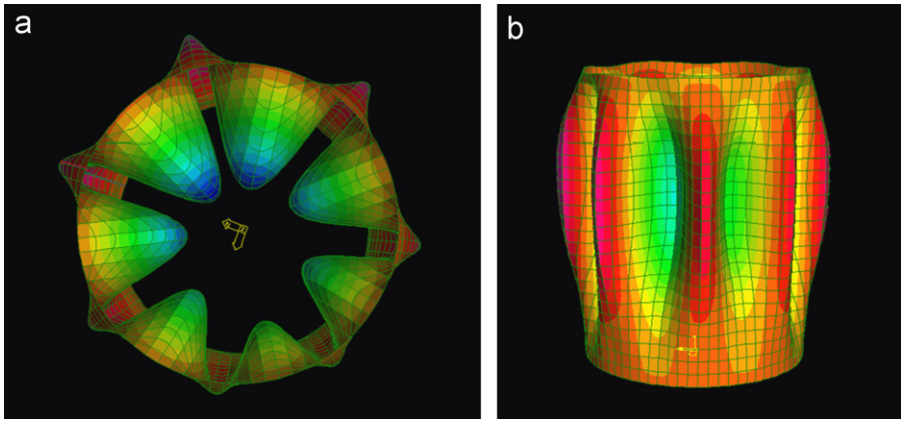

Fig. 18. Predicted mode shape at snap-through, seven lobes. (a) shows plan view and (b) shows elevation. The can ends are removed for visual clarity. Displacements 10 × .

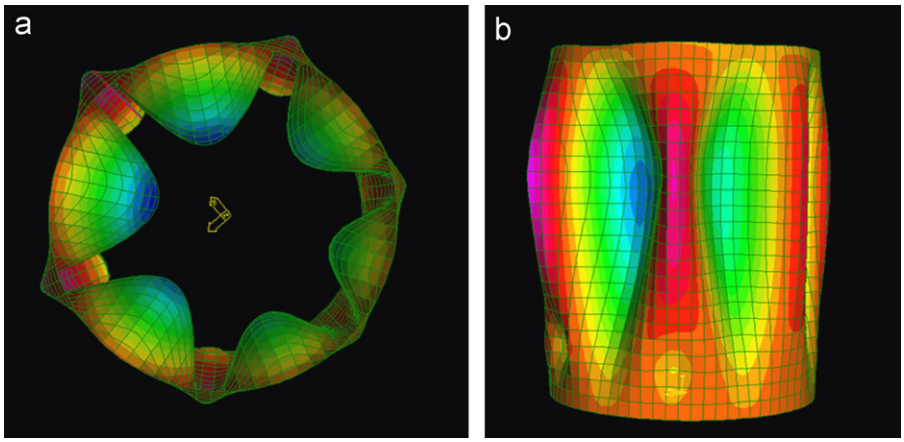

Fig. 19. Snap-through to six lobes predicted by the FE analysis on Can 24. (a) shows plan view and (b) shows elevation. The can ends are removed for visual clarity. Displacements 5 × .

at both ends (at $R=r$ for $Z=0$ and $Z=l$) to represent the geometry of the fold connection. A full geometrically nonlinear static analysis was carried out and it was seen to have no effect on the buckling pressure.

5. Experimental analysis

To validate the FE analysis, five of the measured cans were tested in the laboratory. Each can in the entire collection was assigned a number in the range 1–39. The cans to be tested were chosen at random from the collection and were numbered 12, 17, 24, 28 and 35. Nominal dimensions are given in Table 2. The experimental set-up is as shown in Fig. 14. The cans were simply supported with closed ends. Steam at 100 °C flowed in one end pushing out cooler air through an outlet pipe at the other end. At each end there was a valve and when the can had been filled with steam and the cooler air emptied, the valves were closed. The cans were allowed cool under normal atmospheric conditions in the laboratory. Upon cooling, the steam inside the vessel condensed, creating a uniform vacuum (negative pressure), causing buckling and ultimately the complete collapse of the vessel. Pressure is recorded throughout the experiment using a pressure sensor located inside the can as well as one outside recording ambient pressure. The experimental collapse pressure given in Table 3 is calculated as the difference between the two recorded measurements.

6. Results

Table 3 contains the theoretical results from the Von Mises formula for the buckling of a perfect cylinder subjected to uniform external pressure. The numerical and experimental values for critical pressure for each of the five cans are also presented here. The number of circumferential waves, n, predicted analytically is 8 for each of the cans. However, in the experiments, only six circumferential waves are visible. Fig. 16 shows the deformed shape of the can after testing, while Fig. 15 shows net external pressure which was sampled throughout the experiments plotted against time. It is clear from the pressure histories where the bifurcation point occurs for each can. There is a sharp decrease in pressure, followed by short phase of post-buckling stability, and then total failure of the can. Cans 35 and 24 took longer to collapse than the others as there was a problem with the steam inlet valve. This however does not affect the data.

The numerical analysis initially predicts eight lobes in the elastic stage of the nonlinear analysis (see Fig. 17), and at the bifurcation point where snap-through occurs this number reduces to seven (see Fig. 18). This occurs in the analysis for each of the five cans tested. On further analysis of Can 24, another snap-through event occurs and the number of lobes reduces to six replicating the experiments. This can be seen in Fig. 19. The ends of the can were included in the analysis but removed from Figs. 17 to 19 solely for visual clarity. Fig. 20 shows the force–displacement curve from the FE analysis for each of the cans. The

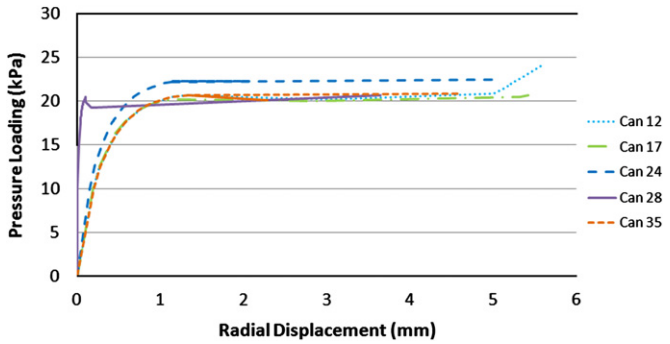

Fig. 20. Force–displacement curve obtained from the FE analysis.

force is obtained from the load which is applied incrementally and the displacement shown is the radial displacement of the node where the greatest deformation occurs.

7. Discussion

On comparing the buckling pressures attained by experiment with those predicted by the FE analysis (see Table 3), excellent correlation is shown. The mean difference in experimental and numerical buckling pressures is 4.77%. These results improve on those found in the literature. Aghajari et al. [2] presented an error of 7–13% between numerical and experimental results, Frano and Forasassi [18] achieved results within 10–15% and Reid et al. [17] presented results with a discrepancy of about 10%. Discrepancies of up to 17% exist between the classical theory prediction of the buckling load and the experimental results. This inconsistency may be attributed to the sensitivity of the experimental buckling loads to imperfection. The classical theory is based on the assumption of a perfect shell and so will give more conservative results than experimental results.

The number of circumferential waves of $n=8$ is predicted both by the theory and the elastic/small-displacements stage of the FE models. This value is higher than the value of $n=6$ noted in the experiments. This difference in wave number is consistent with other experiments where the number of circumferential waves has been less in the experiments than that predicted [11,29]. However, a phenomenon known as mode jumping is evident in the nonlinear FE analysis. This is essentially a dynamic jump where the structure snaps from one mode shape to another to reduce the strain energy. During loading of a structure, the structure reaches a point of instability or a bifurcation point where buckling occurs. At this point, many postbuckling paths may exist in close proximity or may interact with each other (mode interaction). The structure will follow the nearest failure path with the lowest energy level and deform into a particular mode shape. Several paths for different deformation modes may exist within very close range of each other and even overlap, but not all paths that exist at this particular value of the load will be stable. Thus, there is the possibility that the structure may jump from one path to a more stable one where it may come to rest. It is typical that the load will decrease immediately after buckling but may increase again in a later, more stable, postbuckling stage. As the postbuckling mode shape of a shell is highly sensitive to imperfection, this has proven to be very difficult to accurately predict. In the nonlinear analysis for Can 24, eight lobes formed in the initial loading stage, followed by a snap-through to seven lobes, and the solution finally coming to rest at six lobes. Vaziri [30] documented mode jumping in his experiments on highly deformed elastic shells where the displacements and mode changes were clearly visible. In our experiments, the displacements in the loading stage are so small ($\ll 1$ mm) that it is not possible to see them with the naked eye. Thus, we only see the deformed postbuckling shape where $n=6$. These small displacements may be captured in future experimental work using strain gauges (converting strains to displacements) or high resolution photography.

8. Conclusion

An experimental and numerical analysis of the buckling of cylindrical shells under a uniform external loading is presented. Geometric imperfections based on measured data of five cans were modelled in a nonlinear finite element analysis. Buckling collapse experiments were carried out in the laboratory and the results compared. The study shows that the numerical analysis of the buckling process predicted by the FE model closely follows the experimental behaviour, accurately predicting both collapse pressure and deformed shape. It is seen that geometric imperfection clearly reduces the buckling capacity of cylindrical shells subject to uniform external pressure. Despite the structural complexity of the buckling phenomenon, it is seen that buckling behaviour including mode jumping can be satisfactorily predicted using finite element analyses when nonlinearity of the model is taken into account.

Acknowledgments

Thanks go to Paul Conway who helped with the experimental setup and Tim Power and Michael O'Shea who very carefully built the measurement rig. Funding for this research was provided by IRCSET 'Embark Initiative'.

References

[1] Process safety beacon; 2007.
[2] Aghajari S, Abedi K, Showkati H. Buckling and post-buckling behavior of thin-walled cylindrical steel shells with varying thickness subjected to uniform external pressure. Thin-Walled Structures 2006:904–9.
[3] Allen HG, Bulson P. Background to buckling. McGraw-Hill Book Company Limited; 1980.
[4] Arbocz J, Abramovich H. The initial imperfection data bank at the Delft University of Technology, Part 1. Technical Report LR-290, Delft University of Technology, Department of Aerospace Engineering; December 1979.
[5] Southwell R. On the general theory of elastic stability. Philosophical Transactions of the Royal Society of London, Series A 1914:187–244.
[6] Timoshenko SP, Gere JM. Theory of elastic stability. 2nd ed.McGraw-Hill Book Company; 1963.
[7] Weingarten VI, Morgan E, Seide P. Elastic stability of thin-walled cylindrical and conical shells under axial compression. AIAA Journal 1965:500–5.
[8] Koiter W. The effect of axisymmetric imperfections on the buckling of cylindrical shells under axial compression. In: Proceedings koninklijke nederlandse akademie van wetenschappen; 1963. p. 265–79.
[9] Ruiz-Teran A, Gardner L. Elastic buckling of elliptical tubes. Thin-Walled Structures 2008:1304–18.
[10] Wang J, Koizumi A. Buckling of cylindrical shells with longitudinal joints under external pressure. Thin-Walled Structures 2010:897–904.
[11] Guggenburger W. Buckling and postbuckling of imperfect cylindrical shells under external pressure. Thin-Walled Structures 1995:351–66.
[12] Lundquist EE. Strength tests of thin-walled duralumin cylinders in compression. Technical Report TR-473, NACA; 1933.
[13] Wilson WM, Newmark NM. The strength of thin cylindrical shells as columns. Technical Report, The Engineering Experiment Station, University of Illinois; 1933.
[14] Almroth B, Holmes A, Brush D. An experimental study of the buckling of cylinders under axial compression. Experimental Mechanics 1964:263–70.
[15] Vodenitcharova T, Ansourian P. Buckling of circular cylindrical shells subject to uniform lateral pressure. Engineering Structures 1996:604–14.
[16] Khamlichi A, Bezzazi M, Limam A. Buckling of elastic cylindrical shells considering the effect of localized axisymmetric imperfections. Thin-Walled Structures 2004:1035–47.
[17] Reid JD, Bielenberg RW, Coon BA. Indenting, buckling and piercing of aluminum beverage cans. Finite Elements in Analysis and Design 2001: 131–44.

[18] Frano RL, Forasassi G. Experimental evidence of imperfection influence on the buckling of thin cylindrical shell under uniform external pressure. Nuclear Engineering and Design 2009:193–200.
[19] Schenk C, Schuëller G. Buckling analysis of cylindrical shells with random geometric imperfections. International Journal of Non-Linear Mechanics 2003: 1119–32.
[20] Arbocz J. Collapse load calculations for axially compressed imperfect stringer stiffened shells. In: Proceedings of AIAA/ASME/ASCE/AHS 25th SDM conference, part 1; 1984. p. 130–9.
[21] Elishakoff I, Arbocz J. Reliability of axially compressed cylindrical shells with random axisymmetric imperfections. International Journal of Solids and Structures 1982:563–85.
[22] Park T, Kyriakides S. On the collapse of dented cylinders under external pressure. International Journal of Mechanical Sciences 1996:557–78.
[23] Teng J, Lin X. Fabrication of small models of large cylinders with extensive welding for buckling experiments. Thin-Walled Structures 2005:1091–114.
[24] Ventsel E, Krauthammer T. Thin plates and shells. 1st ed.Marcel Dekker Inc.; 2001.
[25] Windenburg DF, Trilling C. Collapse by instability of thin cylindrical shells under external pressure. Transactions of the ASME 1934:819–25.
[26] Strand7 Pty Ltd., Strand7 Online Help, r2.4.2 edition, 2010.
[27] Javidruzi M, Vafai A, Chen J, Chilton J. Vibration, buckling and dynamic stability of cracked cylindrical shells. Thin-Walled Structures 2004:79–99.
[28] Song C, Teng J, Rotter J. Imperfection sensitivity of thin elastic cylindrical shells subject to partial axial compression. International Journal of Solids and Structures 2004:7155–80.
[29] Hornung U, Saal H. Buckling loads of tank shells with imperfections. International Journal of Non-Linear Mechanics 2002:605–21.
[30] Vaziri A. Mechanics of highly deformed elastic shells. Thin-Walled Structures 2009:692–700.